52nd AIAA/ASME/ASCE/AHS/ASC Structures, Structural Dynamics and Materials Conference<BR> 19th
4 - 7 April 2011, Denver, Colorado

AIAA 2011-2142

# Complete bifurcation behaviour of aeroelastic systems with freeplay

G. Dimitriadis*

*University of Liège, Liège, 4000, Belgium*

**Over the last couple of decades, a significant amount of research has been carried out on the aeroelastic behaviour of aeroelastic systems with freeplay. It has been established that such systems can undergo Limit Cycle Oscillations (LCO), both periodic and aperiodic. It has also been shown that several LCOs can occur at the same flight conditions, depending on initial conditions. A lot of the work has been applied to a pitch-plunge airfoil with a control surface and freeplay in the control rotation spring but, even for this simple model, the complete LCO behaviour has not been calculated. In this work, a combined approach using equivalent linearization, a shooting-based numerical continuation scheme and branch following is used to calculate the full bifurcation behaviour of such a system. It is shown that the primary LCO branches depend on the underlying linear systems but that there are two branching points from which secondary periodic solution branches emanate and wrap themselves around the primary branches. Up to 13 different LCOs can coexist at a single flight condition. The system undergoes Hopf, fold, flip and Neimark-Sacker bifurcations and the proposed solution method can identify and all of them.**

## I. Introduction

Freeplay in aeroelastic systems has been of interest for a number of decades. It has been clearly demonstrated that freeplay can result in Limit Cycle Oscillations (LCO) that can have an amplitude significantly greater than the size of the freeplay gap. Wind tunnel experiments to that effect were carried out by many researchers, notably Woolston et al,[1,2] Yang and Zhao,[3] Conner et al,[4] Marsden and Price[5] and others. Consequently, significant research effort has been consecrated to the characterization and prediction of such LCOs for a variety of aeroelastic systems. The effort concerns both the aeroelastic modeling and the solution of the resulting nonlinear equations of motion. Even for simple systems, obtaining a complete picture of all the possible LCOs is challenging.

Numerical continuation holds a lot of promise for solving nonlinear aeroelastic systems, due to its ability to perform branch-following. Once a periodic solution has been calculated, the method can follow the evolution of this LCO with changes in the values of the system parameters, such as airspeed or air density. However, some systems with freeplay display very complex LCO behavior, which can cause the branch-following procedure to fail. Failure can occur, for example, in cases where the LCOs become aperiodic. Furthermore, effective branch following depends on the correct identification and handling of impending bifurcations. For some well-documented bifurcations, such as Hopf, folds or flips, this identification is straightforward. However, the LCO branches of nonlinear systems with freeplay can undergo other bifurcations, such as symmetry-breaking bifurcations, which are much more difficult to identify and handle. Finally, the shooting algorithm is prone to numerical instability because periodicity is not imposed but is the result of a successfully converged Newton-Raphson procedure.[6] Under certain circumstances, such as the presence of several nearby LCO branches, the success of a shooting procedure can depend strongly on the choice of algorithm parameters and starting LCOs.

The purpose of this paper is to propose a three-part procedure to ensure that the full bifurcation behavior of an aeroelastic system with freeplay can be computed from the equations of motion.

*Assistant Professor, Department of Aerospace and Mechanical Engineering, University of Liège, AIAA Member.

## II. Aeroelastic systems with freeplay

The equations of motion of an aeroelastic system with a single freeplay spring can be written as

$$\dot{\mathbf{x}} = \mathbf{A}\mathbf{x} + \mathbf{b}f(x_n) \tag{1}$$

where $\mathbf{x}(t)$ is the $n_s \times 1$ state vector that includes both structural and aerodynamic states, $\mathbf{A}$ is the $n_s \times n_s$ linear system matrix and $\mathbf{b}$ is the $n_s \times 1$ vector coefficient of the nonlinear function. The freeplay spring is attached to state $x_n$ (which must be a structural state); its restoring force is denoted by the function $f(x_n)$, defined as

$$f(x_n) = \begin{cases} Kx_n - \text{sign}(x_n)K\delta & |x_n| > \delta \\ 0 & |x_n| \leq \delta \end{cases} \tag{2}$$

Figure 1 plots the piecewise linear function $f(x_n)$. Inside the freeplay region, which extends from $-\delta$ to $+\delta$, the restoring force is equal to zero and, hence, the spring stiffness is also zero. Outside this region, the spring stiffness is equal to $K$.

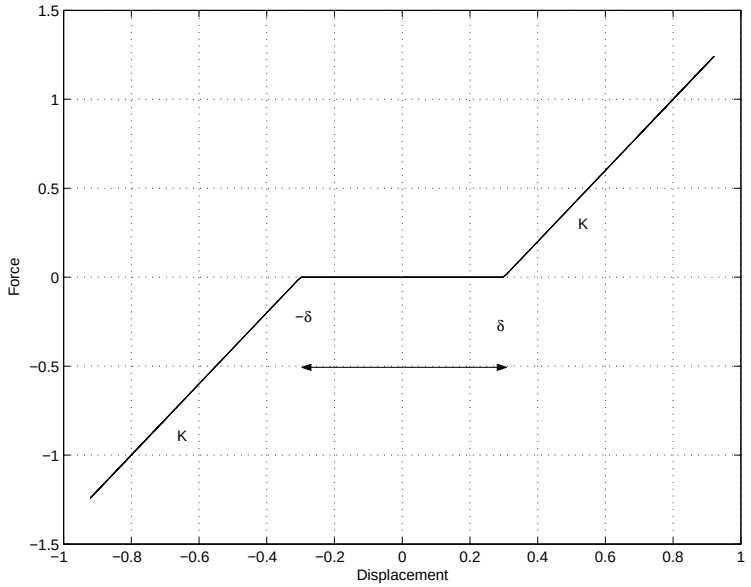


**Figure 1. Freeplay function**

Equation 2 shows that freeplay is, in fact, a combination of two nonlinearities:

- The change in stiffness from 0 to $K$
- The appearance and disappearance of a constant term $-\text{sign}(x_n)K\delta$

The piecewise linear nature of the freeplay spring turns the nonlinear problem of equation 1 into three linear problems in three separate regions of the phase space, which must match at the edges of the freeplay region. The equations of motion can be written as

$$\dot{\mathbf{x}} = \begin{cases} \mathbf{A}_{lin}\mathbf{x} - \mathbf{b}K\delta & x_n > \delta, \text{region } a \\ \mathbf{A}\mathbf{x} & |x_n| \leq \delta, \text{region } b \\ \mathbf{A}_{lin}\mathbf{x} + \mathbf{b}K\delta & x_n < -\delta, \text{region } c \end{cases} \tag{3}$$

where $\mathbf{A}_{lin} = \mathbf{A} + \mathbf{B}$ and $\mathbf{B}$ is a matrix whose entries are all zero except for the $n$th column, which is equal to $\mathbf{b}$. In fact, $\mathbf{A}_{lin}$ is the system matrix of the linear system, i.e. a system for which the width of the freeplay region, $\delta$, is zero.

The response of the nonlinear system is given by the response of the three linear systems in their respective regions, matched at the edges of the freeplay region. As a consequence, the behavior of a system with freeplay depends on two sets of eigenvalues and eigenvectors, those of $\mathbf{A}_{lin}$ and those of $\mathbf{A}$. It also depends on the position of the system's fixed point (i.e. equilibrium point for which $\dot{\mathbf{x}} = \mathbf{0}$

## III. Stability of underlying linear systems

The stability of the systems of equation 3 dictates in a great part the bifurcation behavior of the nonlinear system. Therefore, the first priority is to establish their stability. The aeroelastic example used in the present work is Theodorsen's pitch-plunge airfoil with a nonlinearity in the control surface degree of freedom, with the parameter values used by Tang et al.[7] Figure 2 shows the variation of the damping ratio and natural frequency for the pitch-plunge-control airfoil in regions $a$ and $c$ (the constant terms do not affect the eigenvalues). The figure demonstrates a classical aeroelastic behavior, with a plunge-pitch flutter mechanism. There is only one instability, flutter, occurring at an airspeed of $V = 23.95$m/s. At this airspeed, the plunge degree of freedom becomes unstable. This would be the aeroelastic behavior of the complete system if there was no freeplay.

Figure 3 shows the damping ratio and natural frequency variation for the pitch-plunge-control airfoil in region $b$. The aeroelastic behavior is markedly different to that of figure 2. Firstly, the natural frequency of the control surface is 0Hz at $V = 0$m/s. The flutter mechanism is plunge-control, resulting at a flutter speed of $V = 6.85$m/s, at which the plunge degree of freedom becomes unstable. However, at an airspeed of 13.11m/s, the control degree of freedom combines with the pitch to cause a second flutter condition, at which the pitch becomes unstable. Finally, at $V = 25.91$m/s, the damping ratio of the plunge crosses the zero axis again, to become positive. At higher airspeeds there is only one unstable degree of freedom, the pitch.

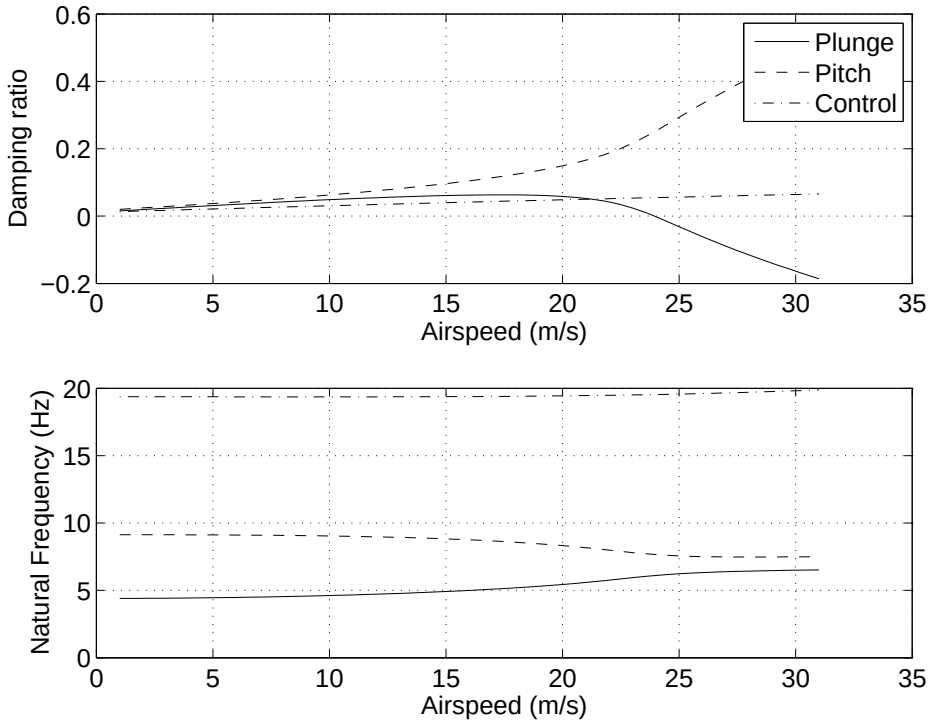


**Figure 2. Damping ratio and natural frequency variation with airspeed for outer linear system**

At all critical airspeeds, one pair of the system eigenvalues is purely complex and therefore purely sinusoidal responses are possible. The phenomenon is known as a degenerate Hopf bifurcation (see for example Strogatz[8]). A degenerate Hopf bifurcation differs from a classical Hopf in the behavior of the system at the Hopf condition. When a classical Hopf bifurcation occurs, a stable focal point becomes unstable and a stable

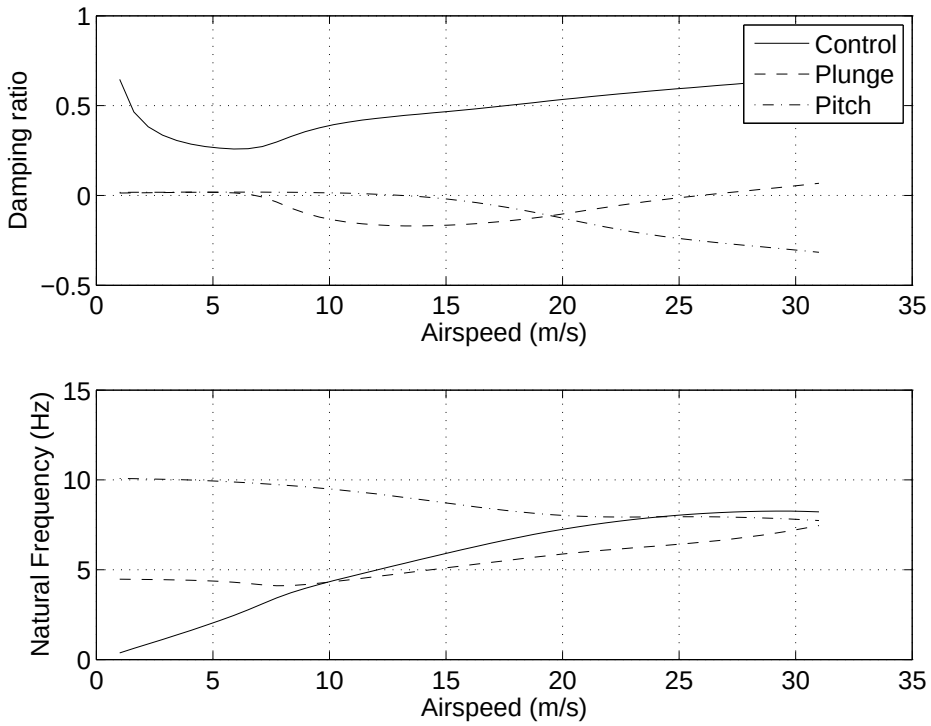


**Figure 3. Damping ratio and natural frequency variation with airspeed for inner linear system**

limit cycle of infinitesimal radius appears around it. In the degenerate case, the stable focal point becomes a center, around which revolves an infinity of neutrally stable closed orbits. This is exactly what happens at the flutter condition of a linear aeroelastic system.

## IV. Equivalent linearization

The concept of equivalent linearization was introduced in aeroelasticity and applied to systems with freeplay in the 1980s, notably by Yang and Zhao.[3] In this work it will be used as a starting point for a more accurate bifurcation prediction method. Equivalent linearization essentially states that, if the response of the nonlinear degree of freedom (dof) is periodic with amplitude $A$, the nonlinear system can be approximated as a linear system with stiffness $K_{eq}$ in the nonlinear dof. Therefore, an approximation of the LCO amplitude versus airspeed plot of the nonlinear system can be obtained. This is shown in figure 4, where $V_{F_1}$ to $V_{F_3}$ denote the the degenerate Hopf bifurcations of the linear system in region $b$ and $V_{F_{lin}}$ denotes the single flutter speed of the linear system in regions $a$ or $c$. Finally, $\beta = \delta$ denotes the boundary of the freeplay region.

There are two branches in the figure 4:

1. A branch starting at the lowest flutter speed of region $b$ and asymptoting to the only flutter speed of region $a$. This branch will be termed branch 1.

2. A branch starting at the control-pitch flutter speed of region $b$ and looping around to the plunge stabilization speed of region $b$. This branch will be termed branch 2.

The frequencies of the LCOs shown in figure 4 can be approximated using the flutter frequencies of the linear system with increasing control stiffness. A plot of flutter frequency against flutter airspeed for the pitch-plunge-control airfoil is shown in figure 5. In this plot, $f_{F_1}$ to $f_{F_3}$ denote all the flutter frequencies of the linear system in region $b$ while $f_{F_{lin}}$ denotes the single flutter frequency of the linear system in regions $a$ or $c$. It can be seen that there are again two branches, one starting at the lowest flutter condition of the

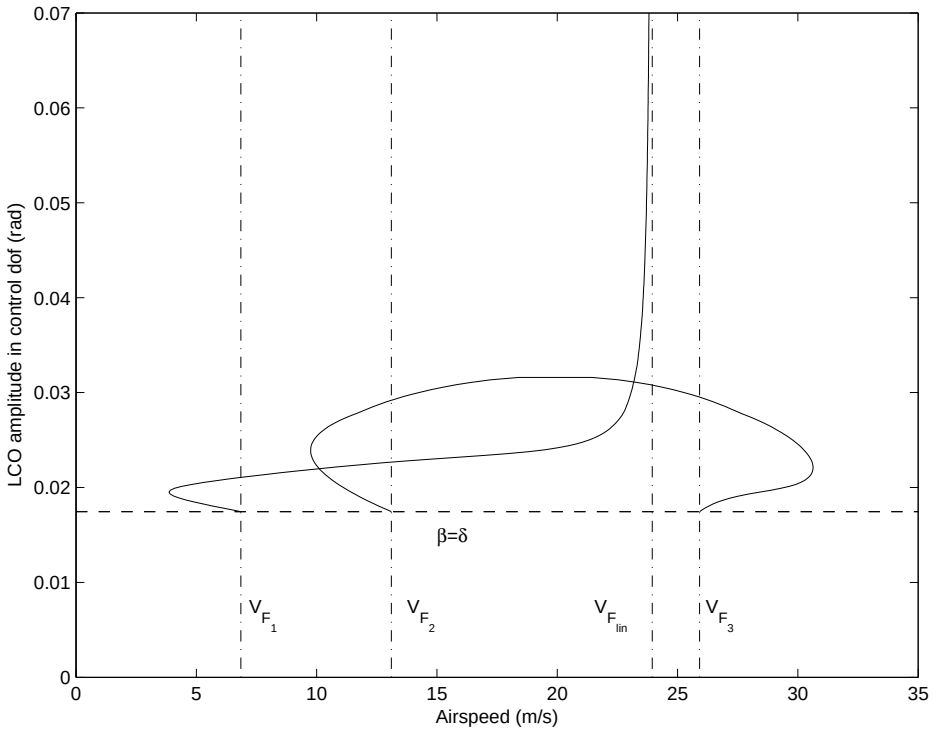


**Figure 4. Variation of LCO amplitude in control dof with airspeed by equivalent linearization**

system in $b$ and ending at the flutter condition of the system in $a$ or $c$ and another connecting the two other flutter conditions of the system in $b$.

## V. Improving the equivalent linearization results

Equivalent linearization approximates a LCO response with a purely sinusoidal response. The true LCO waveforms on the other hand will only be pure sinusoids at the flutter airspeeds of the linear system in region $b$ and at a response amplitude in the control dof equal to $\delta$. At all other conditions, the LCOs will be non-sinusoidal and, in some cases, aperiodic. Therefore, the LCO amplitude and frequency plots of figures 4 and 5 are only a first approximation and can be improved.

In this work, the improvement of the equivalent linearized results is achieved using a shooting approach. As mentioned in the introduction, numerical continuation is a powerful approach for the bifurcation analysis of nonlinear systems. Once a point on an LCO branch has been located, numerical continuation can follow this branch as it evolves with varying values of the system parameters. Furthermore, if the continuation is performed with respect to an arc length parameter, the method can follow branches that undergo further bifurcations, such as folds, period doubling, secondary Hopf bifurcations etc. However, the resulting algorithms are not robust with respect to their numerical parameters. There are several different approaches for carrying out arc length continuation, none of which are universally effective. For example, their results depend on the chosen arc-length step or, in the case of variable step methods, the condition used for step adjustment (e.g. speed of convergence or number of iterations to convergence). Furthermore, additional bifurcations can only be detected if specific tests are carried out; if these tests do not take place the continuation may fail completely. Therefore, at each arc length step, tests for all likely bifurcations must be carried out, introducing further numerical complexities and dependence on additional numerical parameters. Finally, even if a secondary bifurcation is detected, it can be very difficult to follow it.

In this work, the equivalent linearized LCO branch approximations are used as good initial guesses for a numerical continuation analysis. This process does not require branch-following and the algorithm is significantly simplified. Each sinusoidal waveform predicted by equivalent linearization is thus transformed quickly and accurately into a true LCO waveform of the nonlinear system.

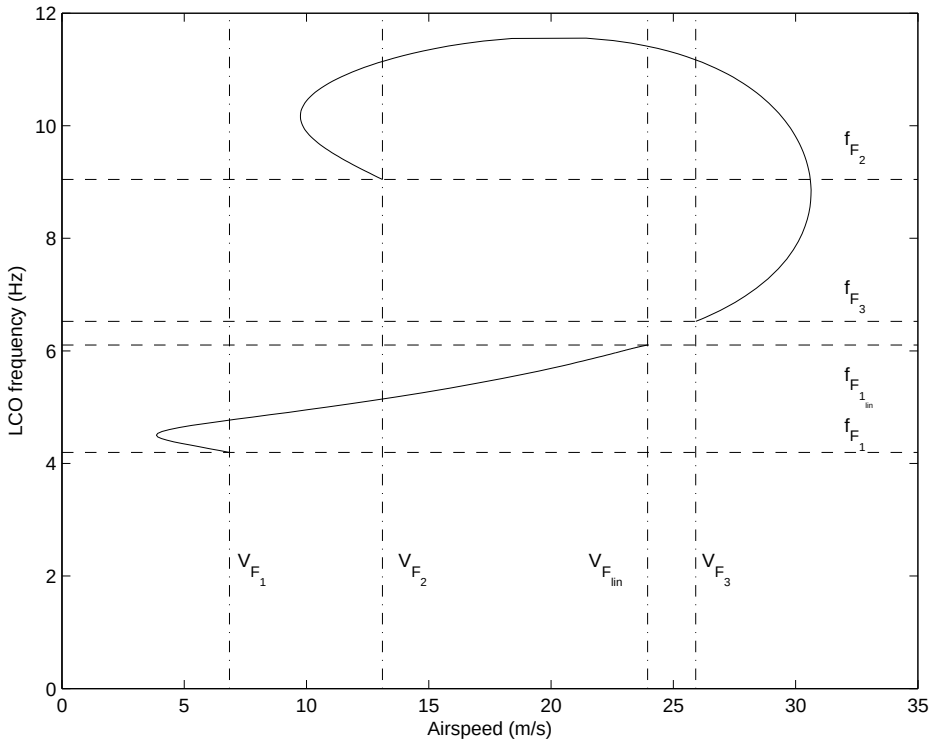


**Figure 5. Variation of LCO frequency with airspeed by equivalent linearization**

## VI. Shooting from equivalent linearized data

Nonlinear numerical continuation solves the nonlinear equations of motion 1 to identify periodic solutions with period, $T$, such that

$$\mathbf{x}(0) = \mathbf{x}(T) \tag{4}$$

The nonlinear ODEs of equation 1 are transformed into a set of nonlinear algebraic equations using a variety of methods, the most popular of which are shooting, finite differences and collocation. For a discussion of the relative merits of shooting and finite differences as applied to aeroelastic systems see Dimitriadis.[6] Nevertheless, systems containing piecewise linear functions cannot be integrated in time with a constant time step, therefore finite differences and collocation are not straightforward to apply to such systems. In this work a shooting approach is used, as applied to self-excited nonlinear aeroelastic systems by Dimitriadis.[9]

The objective of the shooting approach is to minimize the shooting function $\mathbf{F} = \mathbf{x}(0) - \mathbf{x}(T)$ using a Newton-Raphson approach. The procedure is started using a guess for the initial conditions $\mathbf{x}_0(0)$ and period $T_0$, integrating the equations of motion from time 0 to $T_0$, calculating $\mathbf{x}_0(T_0)$ and evaluating the shooting function $\mathbf{F}_0$.Then, better values for $\mathbf{x}_0(0)$ and $T_0$ can be obtained by solving the Newton system

$$\begin{pmatrix} \Delta\mathbf{x} \\ \Delta T \end{pmatrix} = -\begin{pmatrix} \dfrac{\partial \mathbf{F}}{\partial \mathbf{x}(0)} & \dfrac{\partial \mathbf{F}}{\partial T} \end{pmatrix}^{-1} \mathbf{F}_0 \tag{5}$$

and

$$\begin{aligned} \mathbf{x}_1(0) &= \mathbf{x}_0(0) + \Delta\mathbf{x} \\ T_1 &= T_0 + \Delta T \end{aligned}$$

where $\partial\mathbf{F}/\partial\mathbf{x}(0)$ and $\partial\mathbf{F}/\partial T$ are calculated numerically, using a forward difference scheme.

Equations 5 are a set of $n_s$ equations with $n_s+1$ unknowns. A phase-fixing condition can be used in order to balance the number of equations and unknowns. In the present work the phase fixing condition consists of setting one of the initial conditions, for example the last element of $\mathbf{x}(0)$, to be always zero. Therefore, there are $n_s$ equations with $n_s$ unknowns. This type of phase-fixing can cause problems in the case where the LCO is asymmetric and the fixed state cannot pass from zero. The implementation of the method must be flexible enough to change the fixed state under such circumstances.

The numerical integration from time 0 to time $T$ must be carried out using an event-driven approach. The times at which the freeplay region is crossed must be determined with a high degree of accuracy. The approach used here is a Runge-Kutta-Fehlberg 4th-5th order algorithm[10] with backstepping, i.e. every time the freeplay region is crossed, the algorithm moves back a step, divides the time step by 2 and then advances with this new, smaller, time step. The process is repeated until the crossing time is determined to a predefined tolerance; then, the time step is set back to its default value and the algorithm proceeds as normal. The derivatives of equation 5 are calculated numerically.

In a branch-following numerical continuation procedure, the initial guess is obtained from a branch-switching procedure, designed to the take the continuation from, say, an equilibrium solution branch to a LCO branch. Once an accurate point on the LCO branch is calculated, the solution continues to follow this branch for different values of the system parameter.

In the present work, the initial conditions are obtained from the equivalent linearized results. For each set of approximate $\mathbf{x}_0(0)$, $T_0(0)$ and $V_0(0)$ values calculated by equivalent linearization, a new set of converged $\mathbf{x}(0)$, $T(0)$ and $V(0)$ values are estimated using the Newton system

$$\begin{pmatrix} \Delta\mathbf{x} \\ \Delta T \\ \Delta V \end{pmatrix} = -\begin{pmatrix} \dfrac{\partial\mathbf{F}}{\partial\mathbf{x}(0)} & \dfrac{\partial\mathbf{F}}{\partial T} & \dfrac{\partial\mathbf{F}}{\partial V} \end{pmatrix}^{-1} \mathbf{F}_0 \tag{6}$$

and

$$\begin{aligned} \mathbf{x}_1(0) &= \mathbf{x}_0(0) + \Delta\mathbf{x} \\ T_1 &= T_0 + \Delta T \\ V_1 &= V_0 + \Delta V \end{aligned} \tag{7}$$

where, again, $\partial\mathbf{F}/\partial V$ is calculated using a forward difference approach.

Despite the phase-fixing, the system of equations 6 contains more unknowns than equations, due to the addition of the airspeed as an unknown. An additional equation can be obtained by specifying the search direction to be perpendicular to the equivalent linearization LCO branch. Denote by $\mathbf{p}$ a point on this branch such that $\mathbf{p} = [\mathbf{x}_0(0)^T \quad T_0 \quad V_0]^T$. Now consider three such consecutive points on the branch, $\mathbf{p}_{k-1}$, $\mathbf{p}_k$ and $\mathbf{p}_{k+1}$. If the shooting algorithm is applied to point $\mathbf{p}_k$ and the search direction is specified as perpendicular to the branch, then

$$\left(\mathbf{p}_{k+1} - \mathbf{p}_{k-1}\right)^T \Delta\mathbf{p} = 0 \tag{8}$$

where $\Delta\mathbf{p} = [\Delta\mathbf{x}^T \quad \Delta T \quad \Delta V]^T$. This condition is used to complete equations 6 such that

$$\begin{pmatrix} \Delta\mathbf{x} \\ \Delta T \\ \Delta V \end{pmatrix} = \begin{pmatrix} \dfrac{\partial\mathbf{F}}{\partial\mathbf{x}(0)} & \dfrac{\partial\mathbf{F}}{\partial T} & \dfrac{\partial\mathbf{F}}{\partial V} \\ \left(\mathbf{p}_{k+1} - \mathbf{p}_{k-1}\right)^T & & \end{pmatrix}^{-1} \begin{pmatrix} -\mathbf{F}_0 \\ 0 \end{pmatrix} \tag{9}$$

Once a converged LCO is reached, its stability can be assessed by calculating its Floquet multipliers. These are the eigenvalues of the monodromy matrix, $\Phi(T)$. Calculating the monodromy matrix is equivalent to carrying out a shooting calculation,[11] therefore

$$\Phi(T) = -\partial\mathbf{F}/\partial\mathbf{x}(0) + \mathbf{I} \tag{10}$$

where $\mathbf{I}$ is a $n_s \times n_s$ unit matrix. The multipliers of stable periodic solutions all lie on or inside the unit circle. A multiplier outside the unit circle denotes that the solution is unstable, either an unstable limit cycle or an aperiodic orbit.

The complete algorithm is as follows:

1. Calculate a first approximation of the LCO branches using equivalent linearization.

2. Estimate the LCO amplitudes of the other states at each point on the approximate LCO branches. For each of these points create vectors **p** containing initial conditions for the states, period and airspeed information.

3. Treat each branch separately. Apply the Newton system of equation 9 at each point on the branch (apart from the first and last points) until convergence is achieved.

## VII. Results

In this section, the shooting described above is applied to the pitch-plunge-control airfoil. The equivalent linearized LCO branches are evaluated on 333 points, 199 on branch 1 and 134 on branch 2. Figure 6 shows the control dof LCO amplitude variation with airspeed, as calculated by equivalent linearization and shooting. Two elements are of interest; firstly, the amplitudes have changed after the application of the shooting algorithm. The exact LCO amplitudes have been calculated using the shooting approach. Secondly, shooting has characterized the stability of the LCO branches; circles denote stable LCOs while x's denote unstable ones.

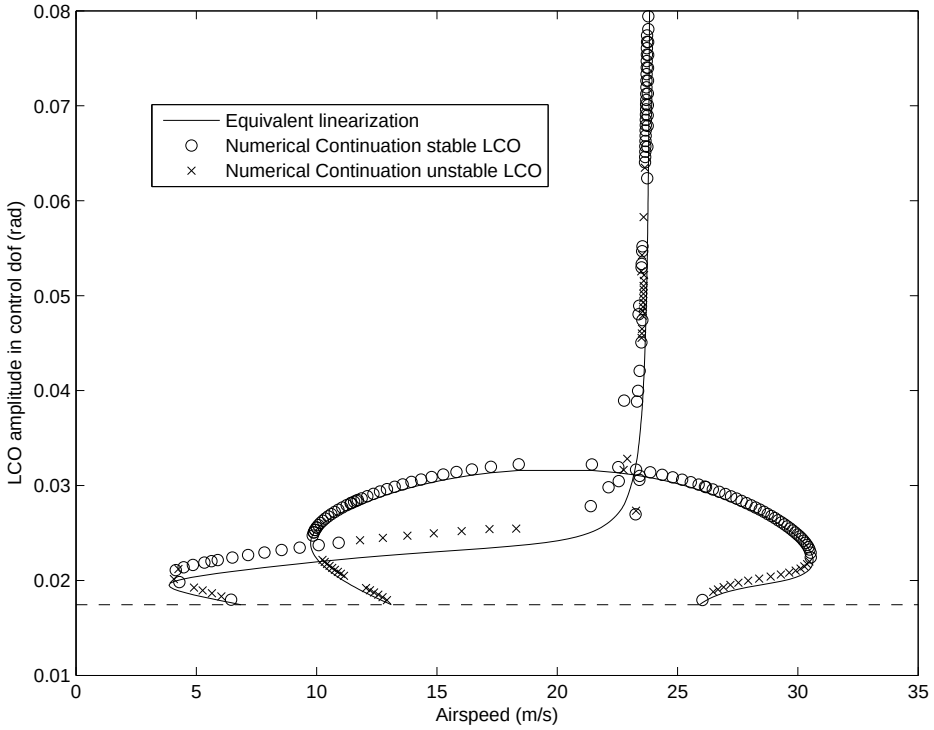


**Figure 6. Comparison of LCO amplitudes by equivalent linearization and shooting**

In the case of figure 6 there are many nearby LCO branches close to the linear flutter speed, $V_{F_{lin}}$. This fact can be seen more clearly by focusing on the first LCO branch between 22 and 24m/s, as shown on figure 7. The shooting approach has identified four LCO branches that intersect near 23.8m/s, three of which are mainly stable while one is mainly unstable. It can be seen that these branches have been calculated intermittently by the algorithm, down to an airspeed of 23.3m/s.

It is of interest to observe the variation of the stability of the LCO branches with airspeed. All branches are unstable immediately after the Hopf bifurcations; they are stabilized by the fold bifurcations. However, the primary LCO branch becomes unstable again after the first intersection with the secondary branch; it is appears to be stabilized again just before the second intersection.

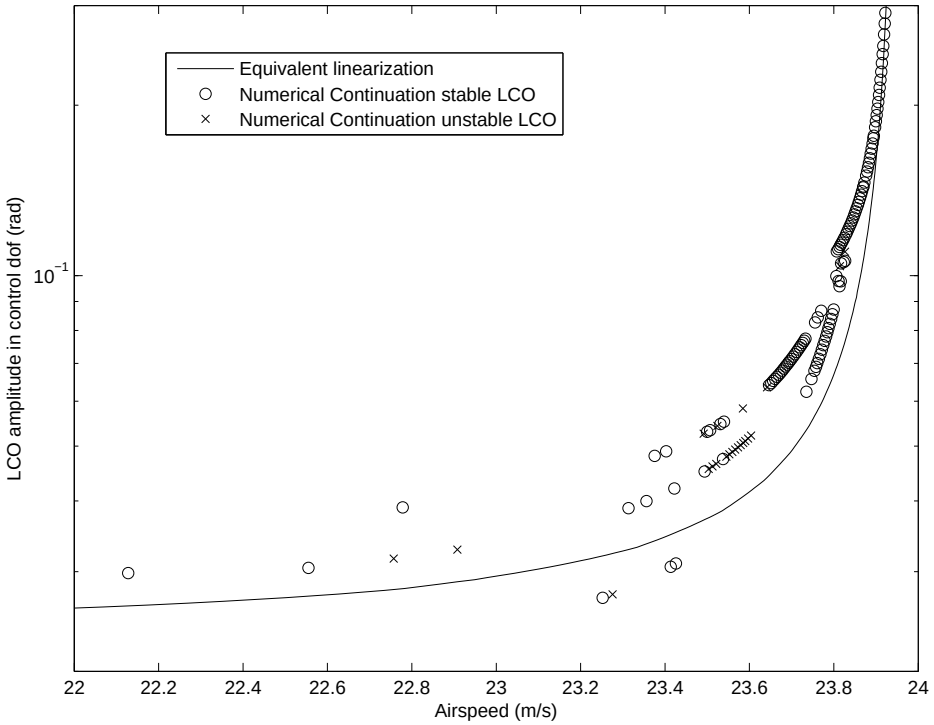


**Figure 7. Comparison of LCO amplitudes by equivalent linearization and shooting between 22 and 24m/s**

## VIII. Post-processing with branch-following numerical continuation

The shooting results of figures 6, although exact, are by no means complete. There are several areas in the parameter space where the number of LCO points is low. Furthermore, the detail of figure 7 shows that several LCO branches have been identified but they are incomplete and it is not clear where they come from.

The bifurcation diagram can be completed by applying branch-following numerical continuation on the periodic solutions already computed. Branch-following applications to aeroelastic systems with freeplay have been described by Dimitriadis[9] and others. The process is similar to that of equations 9 but the closure equation ensures that the numerical continuation procedure is carried out on the same LCO branch, in the direction of an increasing arclength parameter. The pseudo-arclength technique used in the present work can be started from any two nearby periodic solutions in figure 6 that appear to lie on the same LCO branch. The pseudo-arclength parameter, $s$, for these two points can be calculated as

$$\begin{aligned} s_1 &= 0 \\ s_2 &= \sqrt{(\mathbf{x}_2(0)-\mathbf{x}_1(0))^T(\mathbf{x}_2(0)-\mathbf{x}_1(0)) + (T_2-T_1)^2 + (V_2-V_1)^2} \end{aligned}$$

where, here, the subscripts refer to converged values at points 1 and 2. Using these values of $s$, the solution can be projected to the next point on the same branch using linear extrapolation such that

$$\begin{aligned} \mathbf{x}(0) &= \mathbf{x}_2(0) + \frac{\partial \mathbf{x}(0)}{\partial s}\Delta s \\ T &= T_2 + \frac{\partial T}{\partial s}\Delta s \\ V &= V_2 + \frac{\partial V}{\partial s}\Delta s \end{aligned}$$

where $\Delta s$ is a chosen pseudo-arclength increment and

$$\begin{aligned} \frac{\partial \mathbf{x}(0)}{\partial s} &= \frac{\mathbf{x}_2(0) - \mathbf{x}_1(0)}{s_2 - s_1} \\ \frac{\partial T}{\partial s} &= \frac{T_2 - T_1}{s_2 - s_1} \\ \frac{\partial V}{\partial s} &= \frac{V_2 - V_1}{s_2 - s_1} \end{aligned}$$

The values $\mathbf{x}(0)$, $T$ and $V$ are only guesses for the periodic solution at the next point on the branch. They can be refined using a Newton-Raphson approach of the form of equations 9, i.e.

$$\begin{pmatrix} \Delta\mathbf{x} \\ \Delta T \\ \Delta V \end{pmatrix} = \begin{pmatrix} \frac{\partial \mathbf{F}}{\partial \mathbf{x}(0)} & \frac{\partial \mathbf{F}}{\partial T} & \frac{\partial \mathbf{F}}{\partial V} \\ \frac{\partial G}{\partial \mathbf{x}(0)} & \frac{\partial G}{\partial T} & \frac{\partial G}{\partial V} \end{pmatrix}^{-1} \begin{pmatrix} -\mathbf{F}_0 \\ -G_0 \end{pmatrix} \tag{11}$$

where $G_0 = \sqrt{(\mathbf{x}(0) - \mathbf{x}_2(0))^T(\mathbf{x}(0) - \mathbf{x}_2(0)) + (T - T_2)^2 + (V - V_2)^2} - \Delta s$ and the derivatives $\partial G/\partial \mathbf{x}(0)$, $\partial G/\partial T$ and $\partial G/\partial V$ are calculated using a forward difference approach, as with the $\mathbf{F}$ derivatives.

As described earlier, the success of a branch-following procedure depends on the arclength step size $\Delta s$, the parameters of the adaptive step numerical integration algorithm employed, the LCO points used to start the procedure, the complexities of the branch being followed and other factors. To ensure that the branch-following results are as complete as possible, the procedure was applied interactively, choosing points from figure 6 and following the branches on which they lied for as long as the branch-following procedure could advance with the chosen parameters.

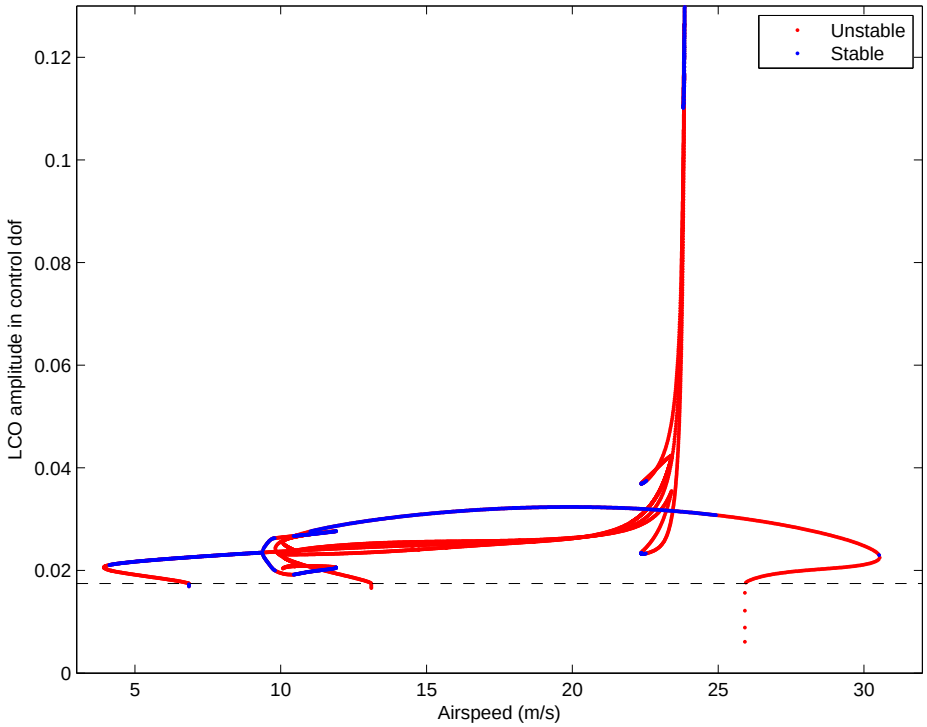


**Figure 8. LCO amplitudes in control d.o.f. by branch-following**

Figure 8 shows the LCO amplitude in the control d.o.f., as calculated using path following from the results of figure 6. The blue dots denote stable LCOs while the red dots denote unstable LCOs. The width of the freeplay region, $\delta$, is denoted by the dashed line. The two main LCO branches identified by the equivalent linearization procedure are clearly present. However, there are two more LCO sub-branches encircling branch

1 near the linear flutter speed and extending down to the first intersection of branches 1 and 2. Figure 9 shows a detail of figure 8 between 9 and 17m/s. At 9m/s branch 1 is stable and symmetric but undergoes a symmetry-breaking bifurcation at 9.4m/s. At this airspeed, branch 1 becomes unstable and two stable sub-branches are created on either side. The upper sub-branch is denoted by $1^+$ and the lower by $1^-$. Such symmetry-breaking bifurcations of periodic solutions can occur in symmetric systems when one real Floquet multiplier exits the unit circle at $+1$.[12] They are also known as pitchfork bifurcations of limit cycles.[11]

By following sub-branches from left to right, it can be seen that they undergo several fold bifurcations, cross over each other and eventually they exchange positions, sub-branch $1^-$ moving above branch 1 and $1^+$ moving below branch 1. Furthermore, in the neighborhood of the intersection between branches 1 and 2, the sub-branches wind themselves around both primary branches.

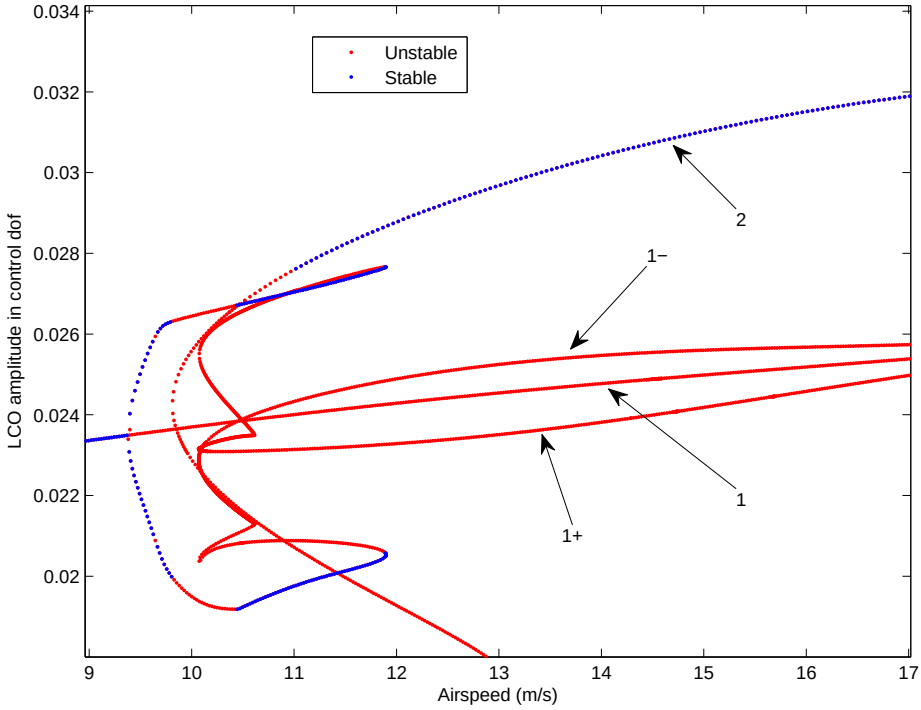


**Figure 9. LCO amplitudes in control d.o.f. by branch-following between 9 and 17m/s**

Figure 10 is a detail of figure 8 in the region between 22 and 24m/s and can be compared to figure 7. It can be seen that branch 1 is still unstable in this region while the two sub-branches undergo a series of folds, becoming briefly stable between 22.4 and 22.5m/s. At around 23.8m/s the three branches merge into one stable branch through a subcritical symmetry-breaking (or pitchfork) bifurcation. The sub-branches disappear and branch 1 becomes stable. It then undergoes a two successive fold bifurcations that form a loop and, finally, it asymptotes towards the linear flutter speed.

Figures 8 to 9 show that the two sub-branches form a closed loop. This loop separates from branch 1 at 9.4m/s and, after winding around both primary branches and undergoing various fold bifurcations, it joins up again with branch 1 at 23.8m/s. It can also be seen as a loop that is generated at 23.8m/s and propagates in the direction of decreasing airspeed until it closes at 9.4m/s. Furthermore, the figures show that there are four airspeed regions at which more than one stable LCO is possible. These regions are

- 9.4-9.8m/s where two stable LCOs are possible, one on each sub-branch,
- 10.4-11.9m/s where three stable LCOs are possible, on branches $1^+$, $1^-$ and 2,
- 22.4-22.5m/s where again three stable LCOs are possible, on branches $1^+$, $1^-$ and 2,
- 23.8-23.9m/s where two stable LCOs are possible, one on branch 1 and one on branch 2.

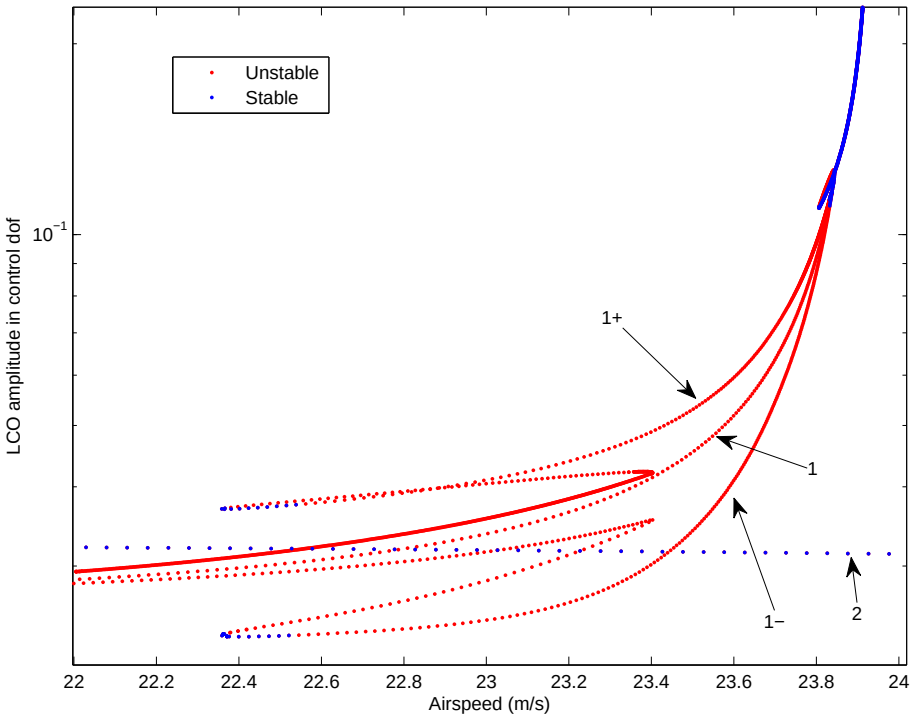


**Figure 10. LCO amplitudes in control d.o.f. by branch-following between 22 and 24m/s**

There is also one airspeed range in which no stable LCOs are possible. This range lies between 9.8m/s and 10.4m/s and only aperiodic LCOs can occur within it. Any numerical integrations started on any of the unstable limit cycles will move away from the LCO, settling eventually on an aperiodic oscillation. This phenomenon is due to a Neimark-Sacker bifurcation occurring on the two sub-branches at around 9.8m/s. A Neimark-Sacker (or torus) bifurcation occurs when a periodic solution on a limit cycle becomes a quasi-periodic solution on a torus and is characterized by a pair of complex conjugate Floquet multipliers exiting the unit circle.[11–13] This pair of eigenvalues re-enters the unit circle at around 10.4m/s, causing a subcritical Neimark-Sacker bifurcation; the sub-branches become stable limit cycles again. In the airspeed range between the supercritical and subcritical Neimark-Sacker bifurcations the system can only undergo aperiodic LCOs; no stable periodic solutions are possible. It is interesting to note that the first Neimark-Sacker coincides with the intersection of LCO branches 1 and 2, although it is not clear what exactly the effect of this intersection is on the sub-branches.

Figure 11 shows the variation of the fundamental frequencies of the LCOs, as calculated using the branch-following approach. These frequency values can be compared to those of figure 5, which were calculated by equivalent linearization. It can be seen that the two sets of frequencies are very similar; the main differences lie in the existence of the LCO sub-branches, which wind around branch 1 between 9.4m/s and 23.8m/s. Nevertheless, the frequencies of the sub-branches are very close to those of branch 1. The comparisons between the equivalent linearization and shooting with branch following estimates of the LCO amplitude and frequency (i.e. figures 4 and 8 for amplitude and figures 5 and 11 for frequency) demonstrate that the mathematical basis of the approach proposed here is sound; the equivalent linearized predictions are good enough to be used as initial guesses for the shooting and branch following procedures. Furthermore, the figures demonstrate the necessity of carrying out the latter stages of the methodology. While equivalent linearization can give good estimates of the LCO amplitudes and frequencies of the two primary branches, it cannot estimate the sub-branches. Furthermore, it cannot determine the stability of the two primary LCO branches with accuracy. According to equivalent linearization, branch 1 is stable from 4m/s to the linear flutter speed and branch 2 is stable between the two folds. Shooting and branch following demonstrate that the stability of the system is far more complicated. Finally, it should be stressed that equivalent linearization

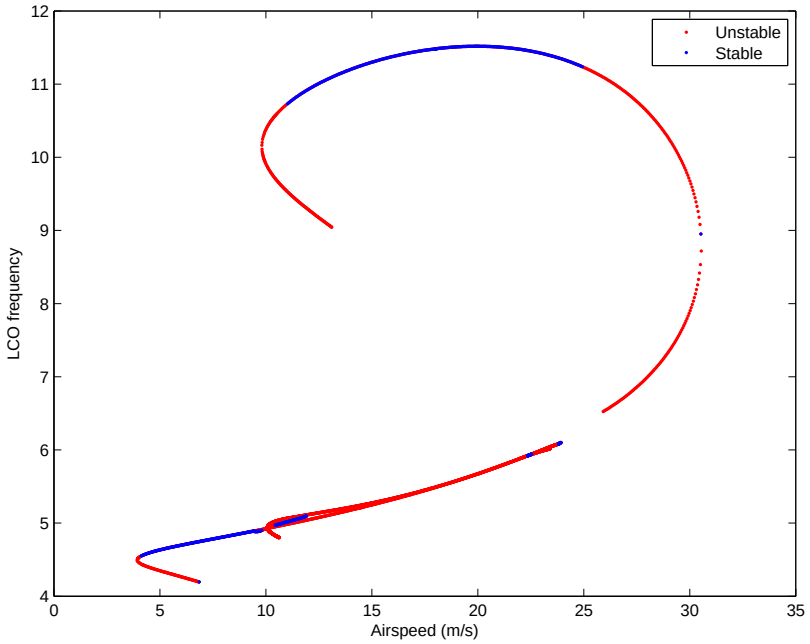


**Figure 11. LCO frequencies in control d.o.f. by branch-following**

cannot predict or explain the appearance of quasi-periodic or aperiodic responses.

The aperiodic responses occurring in the 9.8-10.4m/s airspeed range are of particular interest. Figure 12 shows a Poincaré section of a response at 10.1m/s. The section was obtained after numerically integrating the system from an initial condition on branch 1. The integration was carried out over 240s and the section was drawn at time instances when the control degree of freedom is equal to $+\delta$. The 'pitch displacement - pitch velocity' section (figure 12(a)) shows that the system response lies on two groups of four ovals. Figure 12(b) zooms in on one of these ovals. The Poincaré section of a simple stable limit cycle is two points; that of a response lying on a torus is two ovals. The section of figure 12(a) demonstrates that this particular response lies on a very complex torus, which crosses the 'pitch displacement - pitch velocity' plane eight times. The complexity of the torus is due to the fact that the Neimark-Sacker bifurcation took place after two successive flip (period doubling bifurcations). Each of the flips double the number times the limit cycle crosses the plane, finally resulting in 8 intersections. After the Neimark-Sacker bifurcation, the 8 point intersections became 8 ovals. Most of the oscillations that can take place in this airspeed range have a similar Poincaré section and are therefore aperiodic but not chaotic.

Seydel[11] states that one of the routes to chaos is the Ruelle-Takens-Newhouse route, which is characterized by a Hopf bifurcation, followed by a bifurcation to a two-frequency torus. The torus shown in figure 12(a) has four frequencies and therefore suggests that chaotic oscillations may be possible in this airspeed range. A Poincaré section was also generated for a response with initial conditions on branch $1^-$ at 10.1m/s, just before the branch's second fold. It can be seen that this section also contains two groups of four ovals but, in this case, the ovals have started to either break up or merge together. The detail of figure 13(b) clearly shows that the two ovals have opened up and one of them has a long tail that connects it to another oval on the other side of the plane. This type of Poincaré section is typical of a chaotic response or, at least, of a transition to chaos. Aperiodic and chaotic responses can also occur in the 23-24m/s airspeed range, when the initial conditions lie on branches 1, $1^-$ and $1^+$.

The behavior of branch 2 is also of interest; it undergoes a fold bifurcation just after its intersection with branch 1 but it is not stabilized as a result of the fold. Figure 14 shows the evolution of the Floquet multipliers between the airspeeds of 10 and 12.2m/s. After the degenerate Hopf bifurcation at 13.11m/s, branch 2 is unstable and evolves in the decreasing airspeed direction. One of the Floquet multipliers is real and greater than one. In figure 14 this multiplier lies at 4.2 at an airspeed of 10m/s. All the other multipliers lie inside the unit circle. As the airspeed decreases further, the unstable multiplier travels towards the unit

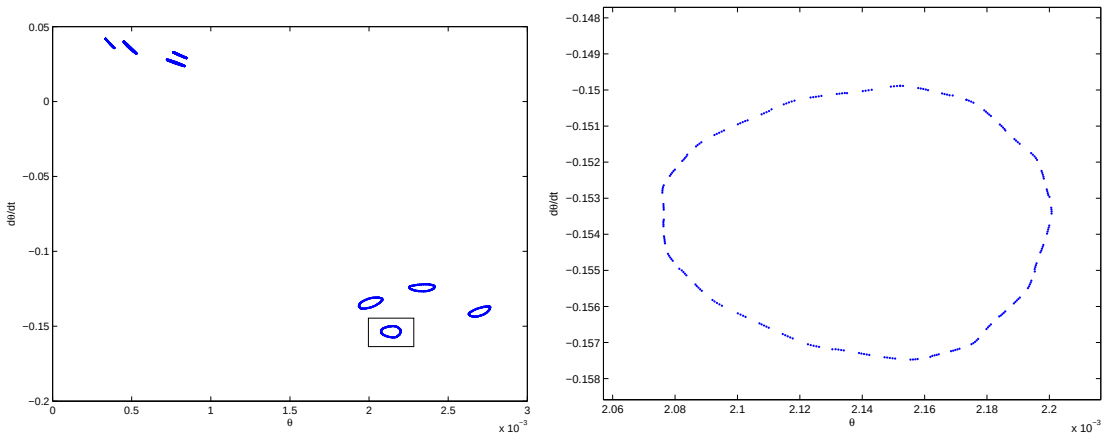


(a) Poincaré section (b) Detail of Poincaré section

**Figure 12. Poincaré section of aperiodic response at 10.1m/s, starting on branch 1**

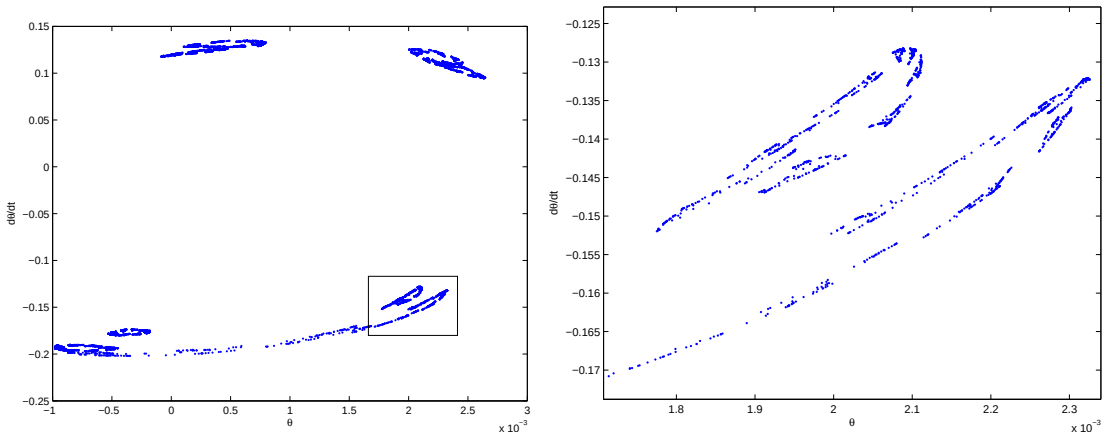


(a) Poincaré section (b) Detail of Poincaré section

**Figure 13. Poincaré section of aperiodic response at 10.1m/s, starting on branch $1^-$**

circle. However, another real multiplier exits the unit circle at the fold at 9.8m/s and collides with the original unstable multiplier. As the the LCO branch starts to move in the increasing airspeed direction, the two multipliers become a complex conjugate pair that moves off the real axis and eventually enters the unit circle at 11.8m/s. Therefore, branch 2 is stabilized as a consequence of a subcritical Neimark-Sacker bifurcation. It becomes unstable again through a supercritical Neimark-Sacker bifurcation at 24.03m/s, i.e. at the flutter speed of the system without freeplay.

## IX. Conclusions

Even though the aeroelastic system studied in this work is simple, it demonstrates a rich bifurcation behavior; it features two main LCO branches and two sub-branches, which are the result of a symmetry-breaking bifurcation on the primary branch. In order to calculate the sub-branches, a traditional branch-following approach would require a complete mathematical description of this symmetry-breaking bifurcation. However, the approach proposed in this work was capable of calculating the complete bifurcation behavior without such a description. In essence, it is accepted that branch-following works best when a partial set of periodic solutions of a system is already known. Therefore, before applying branch-following, a combination of equivalent linearization and shooting is used in order to obtain a cloud of LCO points that belong to all

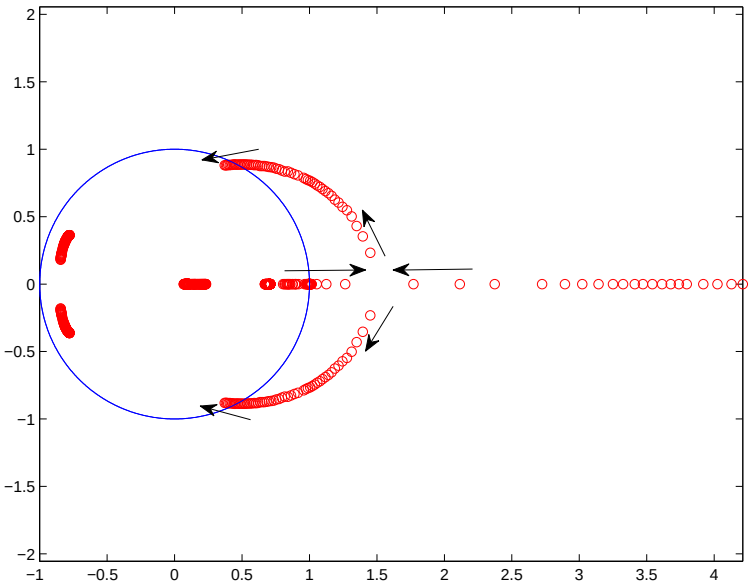


**Figure 14. Floquet multipliers of branch 2 for airspeeds between 10 and 12.2m/s.**

the branches and sub-branches. From then on, branch-following becomes a much more effective process.

The results obtained from the application of the method show that, for this system, the LCO behavior follows in general the two periodic solution branches identified by equivalent linearization. However, the complete calculation of the sub-branches has allowed the observation and explanation of several phenomena that cannot be predicted by linearized analysis. These include several airspeed ranges where more than one LCO are possible as well as occurrences of aperiodic and chaotic responses. The system undergoes degenerate and subcritical Hopf, fold, flip and Neimark-Sacker bifurcations. This combination of phenomena can lead to periodic solutions lying on cycles, tori and strange attractors.

## References

[1]Woolston, D. S., Runyan, H. L., and Byrdsong, T. A., "Some effects of system nonlinearities in the problem of aircraft flutter," Technical Note TN 3539, NACA, Oct. 1955.

[2]Woolston, D. S., Runyan, H. L., and Andrews, R. E., "An investigation of effects of certain types of structural nonlinearities on wing and control surface flutter," *Journal of the Aeronautical Sciences*, Jan. 1957, pp. 57–63.

[3]Yang, Z. C. and Zhao, L. C., "Analysis of limit cycle flutter of an airfoil in incompressible flow," *Journal of Sound and Vibration*, Vol. 123, No. 1, 1988, pp. 1–13.

[4]Conner, M. D., Tang, D. M., Dowell, E. H., and Virgin, L., "Nonlinear behaviour of a typical airfoil section with control surface freeplay: a numerical and experimental study," *Journal of Fluids and Structures*, Vol. 11, 1997, pp. 89–109.

[5]Marsden, C. C. and Price, S. J., "Transient and limit cycle simulation of a nonlinear aeroelastic system," *Journal of Aircraft*, Vol. 44, No. 1, 2007, pp. 60–70.

[6]Dimitriadis, G., "Numerical Continuation of Aeroelastic Systems: Shooting vs Finite Difference Approach," *RTO-MP-AVT-152 Limit Cycle Oscillations and Other Amplitude-Limited Self-Excited Vibrations*, No. AVT-152-025, Loen, Norway, May 2008.

[7]Tang, D., Dowell, E. H., and Virgin, L. N., "Limit cycle behaviour of an airfoil with a control surface," *Journal of Fluids and Structures*, Vol. 12, No. 7, 1998, pp. 839–858.

[8]Strogatz, S. H., *Nonlinear Dynamics and Chaos: With Applications to Physics, Biology, Chemistry, and Engineering*, Perseus Books, Cambridge, MA, 1994.

[9]Dimitriadis, G., "Bifurcation Analysis of Aircraft with Structural Nonlinearity and Freeplay Using Numerical Continuation," *Journal of Aircraft*, Vol. 45, No. 3, 2008, pp. 893–905.

[10]Gerald, C. F. and Wheatley, P. O., *Applied Numerical Analysis*, Addison-Wesley, 5th ed., 1990.

[11]Seydel, R., *Practical bifurcation and stability analysis*, Springer, New York Dordrecht Heidelberg London, 3rd ed., 1994.

[12]Leine, R. I. and Neijmeijer, H., *Practical bifurcation and stability analysis*, Springer Verlag, Berlin Heidelberg New York, 2004.

[13]Kuznetsov, Y. A., *Elements of Applied Bifurcation Theory*, Springer, New York Berlin Heidelberg, 2nd ed., 1998.